Engineered Science
DOI: https://dx.doi.org/10.30919/es1113

Rose-derived Porous Carbon and In Situ Fabrication of Cobalt/Nickel Nanoparticles Composites as High-Performance Electromagnetic Wave Absorber

Wentao Yu,[1] Ziqing Wang,[1] Jiahui Lin,[1] Yongshuang Xiao,[1] Liying Zhu,[1] Jintao Huang,[1,*] Aricson Pereira,[2] Zhanhu Guo[3,*] and Yonggang Min[1,*]

Abstract

Rose-derived porous carbon and Cobalt(Co)/Nickel(Ni) nanoparticles composite absorbers (RC/Co and RC/Ni) were synthesized adopting a simple impregnation method and one-step carbonization method. The special array structure on the surface of rose petals remains intact even after carbonization, and the wrinkles and porous structure inside serves to reduce the material's density and increase the number of interfaces. Besides, the in Situ Fabricated Co and Ni magnetic nanoparticles were employed to introduce magnetic loss ability. At a matching thickness of 1.58 mm, RC/Co exhibits a minimum reflection loss (RL_{min}) of -47.89 dB at 13.60 GHz and an effective attenuation bandwidth (EABW) of 4.08 GHz, while RC/Ni achieves a RL_{min} value of -45.36 dB at 12.88 GHz and an EABW of 3.02 GHz at thickness of 1.56 mm. Due to the low-cost biomass materials and simple preparation methods, RC/Co and RC/Ni could serve as a model for synthesizing other high-performance absorbers due to their environmental friendliness, convenience of synthesis, and good electromagnetic wave (EMW) attenuation capability.

Keywords: Biomass carbon; Rose petals; Porous carbon; Electromagnetic wave absorption.
Received: 04 March 2024; Revised: 18 March 2024; Accepted: 20 March 2024.
Article type: Research article.

1. Introduction

As 5G communications continue to advance and electronic products become increasingly ubiquitous, there is growing public concern regarding the potential electromagnetic wave (EMW) pollution that may result.[1-3] However, the EMW or radiation emitted by electronic equipment can lead to electromagnetic pollution,[4] disrupting the normal functioning of electronic facility and potentially affecting human health.[5] This underscores the pressing need for EMW absorbing materials capable of efficiently absorbing and attenuating EMW.

Traditionally, numerous compounds such as magnetic metal particles (Fe, Co, Ni),[6-8] ferrites (Fe_3O_4, $CoFe_2O_4$, $NiFe_2O_4$),[9-12] dielectric materials[13-17] can function as ideal EMW absorption materials. However, factors such as high density, susceptibility to corrosion, weight, or low absorption have constrained their practical implementation as EMW-absorbing materials. In a broad context, exceptional EMW absorption materials demonstrate robust EMW attenuation capabilities, a wide effective absorption frequency bandwidth, lightweight structures, and thin thicknesses. However, the specific characteristics may vary depending on distinct application conditions.

In contrast to conventional materials, carbon materials such as graphene, reduced graphene oxide and carbon nanotube have garnered attention from the scientific community due to their lighter weight, higher electrical loss, and good chemical stability,[18-21] making them suitable for specific operating environments. However, constructing carbon materials with complex structures and their composite materials often requires precise design, cumbersome processes, and strict reaction conditions.[22,23] These constraints not only hinder the preparation of high-performance EMW absorption

[1] *School of Materials and Energy, Guangdong University of Technology, Guangzhou 510006, China.*
[2] *Engineered Multifunctional composites (EMC) nanotech LLC, Knoxville, TN,37996, United states.*
[3] *Department of Mechanical and Civil Engineering, Faculty of Engineering and Environment, Northumbria University, Newcastle Upon Tyne NE1 8ST, UK.*
**Email:* jintao.huang@gdut.edu.cn (J. Huang), zhanhu.guo@northumbria.ac.uk (Z. Guo), ygmin@gdut.edu.cn (Y. Min)

© Engineered Science Publisher LLC 2024

materials but also pose challenges for large-scale production and applications. Therefore, there is an urgent need for the development of low-cost, simple preparation, environmentally friendly EMW absorption materials with high EMW attenuation capability.

Compared to carbon sources such as coal and petroleum (polymers), biomass is widely present in nature. It is a green, sustainable, and widely applicable raw material of carbon materials.[24-26] Moreover, biomass has its own unique pore structure, and more micropores/mesopores are formed during carbonization as the carbon skeleton shrinks during pyrolysis or fracture, which not only enhances its specific surface area and transmission efficiency, but also leads to improved impedance matching by bring in low-dielectric air in the material.[27-29] Drawing from this design concept, rose petals with distinctive surface morphology were ideal object as a carbon matrix. A biomass porous carbon/magnetic composite EMW absorber was synthesized by pretreating with a salt solution followed by high-temperature carbonization. The corresponding attenuation mechanism was extensively investigated. The findings reveal that the synthesized material demonstrates robust EMW attenuation capabilities across a broad frequency range. Thus, the proposed method offers a rapid and convenient approach for synthesizing high-performance EMW absorbers.

2. Experimental section

2.1 Chemical and materials

Cobalt chloride hexahydrate ($CoCl_2 \cdot 6H_2O$) and nickel chloride hexahydrate ($NiCl_2 \cdot 6H_2O$) (Aladdin Chemistry Co. Ltd) were all used as received. Deionized water was used throughout the experiments. Dried rose petals were supplied by Guangkuntang Agricultural Technology Co., Ltd.

2.2 The synthesis of the rose-derived carbon/Co and Ni nanoparticles composite (RC/Co and RC/Ni)

Firstly, the dry rose petals were immerse in a 60 °C deionized water bath for 1 hour to remove surface and internal foreign substance (pigments, aromatics, *etc*) and dried in an 80 °C oven for 2 hours. Then, as shown in Fig. 1, 3.0 g rose petals were soaked in 100 ml, 0.5mol/L concentration $CoCl_2.6H_2O$ solution at 25 °C for 24 hours under magnetic stirring. Then, the rose petals were thoroughly dried in an 80 °C vacuum oven for 12 hours. Finally, the $CoCl_2$-induced rose petals was calcined in a tubular furnace under the flow of argon gas under specific heating conditions (25 °C – 1000 °C, 5 °C/min; 1000 °C/1 hours). Thus, obtained composites was labelled as RC/Co. The whole preparation process of RC/Ni composite is basically the same as that of RC/Co. 3.0 g rose petals was soaked in 100 ml, 0.5mol/L concentration $NiCl_2.6H_2O$ solution at 25 °C for 24 hours under magnetic stirring. Then, the rose petals were thoroughly dried in an 80 °C vacuum oven for 12 hours. Then the $NiCl_2$ treated rose petals was calcined in a tubular furnace with an argon atmosphere and under the following heating program (25 °C–1000 °C, 5 °C/min; 1000 °C/1 hours).

3. Characterization section

3.1 Characterization methods

The chemical structures of samples were analyzed using X-ray powder diffraction (XRD, D/MAX-Ultima IV, Cu Kα, 10–80°, 10°/min), Raman spectroscopy (LabRAM HR Evolution,523nm laser), Fourier transform infrared spectroscopy (FT-IR, Nicolet6700). The morphology of synthesized materials was determined using scanning electron microscopy (SEM, Nova Nano 450) and energy-dispersive X-ray spectroscopy (EDS, Oxford X-Max system). The electromagnetic parameters (complex permeability and permittivity) were measured using a network analyzer (N5244A PNA-X, Agilent, toroidal-shaped samples with 35 wt% of products in a paraffin wax matrix, coaxial waveguide method, frequency range: 2–18 GHz). The magnetization was measured using a vibrating sample magnetometer (VSM, Lake Shore 7404, 298 K).

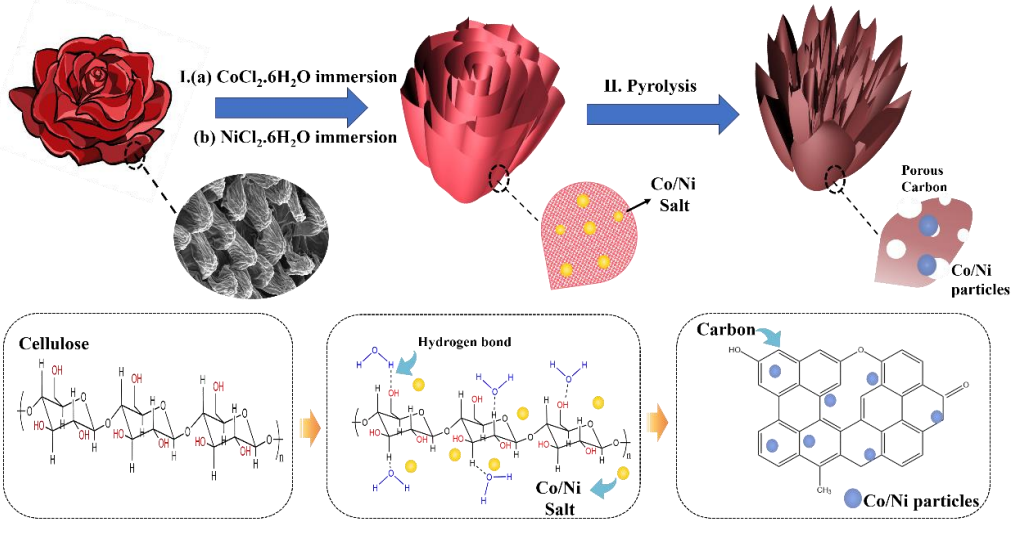

Fig. 1 Synthetic route for the rose-derived porous carbon/Co and Ni nanoparticles composite (RC/Co and RC/Ni).

© Engineered Science Publisher LLC 2024

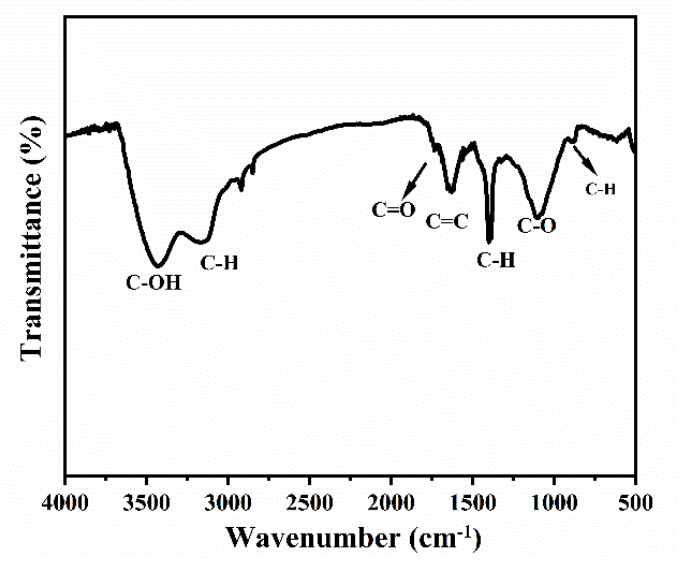

Fig. 2 FTIR spectra of rose petals.

3.2 Results and discussion

The FTIR spectrum displays the components of rose petals, as shown in Fig. 2. The absorption peaks at 3400 cm^{-1} and 3100 cm^{-1} correspond to the stretching vibrations of cellulose O-H and C-H bonds, respectively; The peaks around 1600 cm^{-1} and 1460 cm^{-1} represent the C=C stretching vibration within the aromatic ring of lignin and the -CH_2 deformation vibration on the skeleton, respectively; The peak at around 1100 cm^{-1} represents the symmetric stretching vibration of C-O.

To conform the chemical composition of RC/Co and RC/Ni the XRD pattern was acquired. the characteristic peaks at 75.90°, 51.36°, and 44.12° in XRD patterns in Fig. 3(a) are associated with (220), (200), and (111) planes of Ni (PDF#04–0850); The characteristic peaks at 75.80°, 51.52°, and 44.21° are detected as the same planes of the Co (PDF#15–0806).[30] Besides, RC/Co and RC/Ni exhibit a broad diffraction peak at 23°–27°, ascribed to the (002) plane of amorphous carbon. The above results indicate that RC/Co and RC/Ni composites are successfully synthesized with metallic Co, Ni nanoparticles and amorphous carbon which are key element for absorption of electromagnetic wave (EMW) absorption. The prominent peaks in the Raman spectra in Fig. 3(b) at around 1360 cm^{-1} and 1590 cm^{-1} are attributed to the D and G bands of carbon materials. The intensity ratio of the D/G bands for RC/Co and RC/Ni is 0.97 and 0.96 respectively. indicating that the carbon matrix is mainly composed of amorphous carbon which is conducive to inducing defect polarization. These defects contribute to scattering of electromagnetic wave and promote interfacial polarization, leading to dramatically increase EMW absorption.[31]

The morphology structure of rose petals and Synthesized RC/Co, RC/Ni composites can be observed by SEM. As shown in Fig. 4, Several arrays shaped polygonal protrusions with a length/width of about 5-6 μm can be observed on the surface of the rose petals, and the surface of the protrusions is covered with wrinkles. After salt solution immersion treatment, it was found that the array arrangement on the surface of the petals was disrupted, but the structural unit structure remained intact. After carbonization, the structural units undergo dehydration and contraction into flakes, while the surface still maintains grooves. Additionally, pores with a diameter ranging from 500 nm to 900 nm are formed on the surface due to the collapse of the carbon skeleton Which can increase the specific surface area of composite and trigger multiple scattering of electromagnetic waves inside. Furthermore, it can be observed that there is Co, Ni nanoparticles on the surface of the structural units. According to Figs. 4(h), (i), the EDS element mapping of RC/Co and RC/Ni prove the random distribution of Co, Ni nanoparticles in the porous carbon matrix. The diameter of Co nanoparticles is 800-900 nm, and Ni nanoparticles is 350-800 nm.

To identify the difference in magnetization between Co and Ni, the M-H loops of RC/Co and RC/Ni were shown in Fig. 5. the remanent magnetization (Mr) of RC/Co and RC/Ni were 8.80 $emu \cdot g^{-1}$ and 6.44 $emu \cdot g^{-1}$ respectively. Besides, the low nonzero coercivity (Hc) of RC/Co and RC/Ni (26.65 Oe and 48.64 Oe) mean the super paramagnetic property of the Co and Ni nanoparticles.

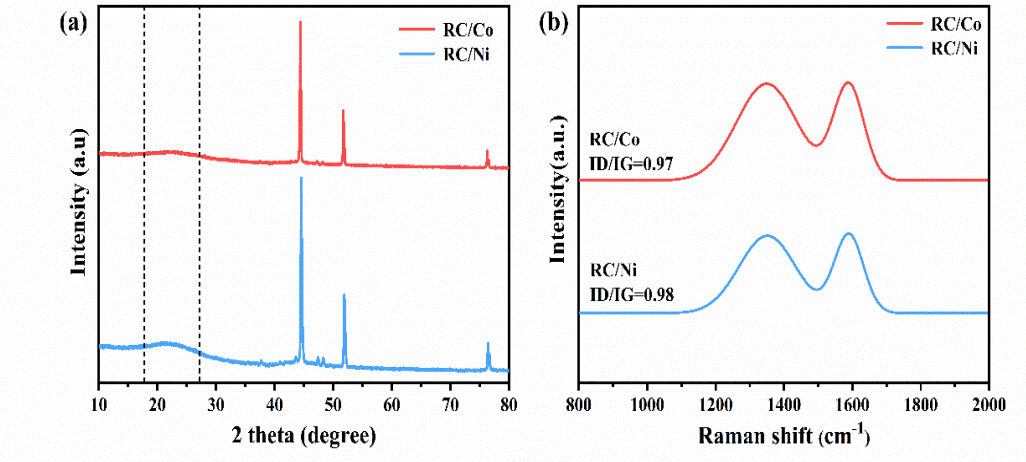

Fig. 3 (a) XRD patterns of RC/Co and RC/Ni; (b) Ramen spectra of RC/Co and RC/Ni.

© Engineered Science Publisher LLC 2024

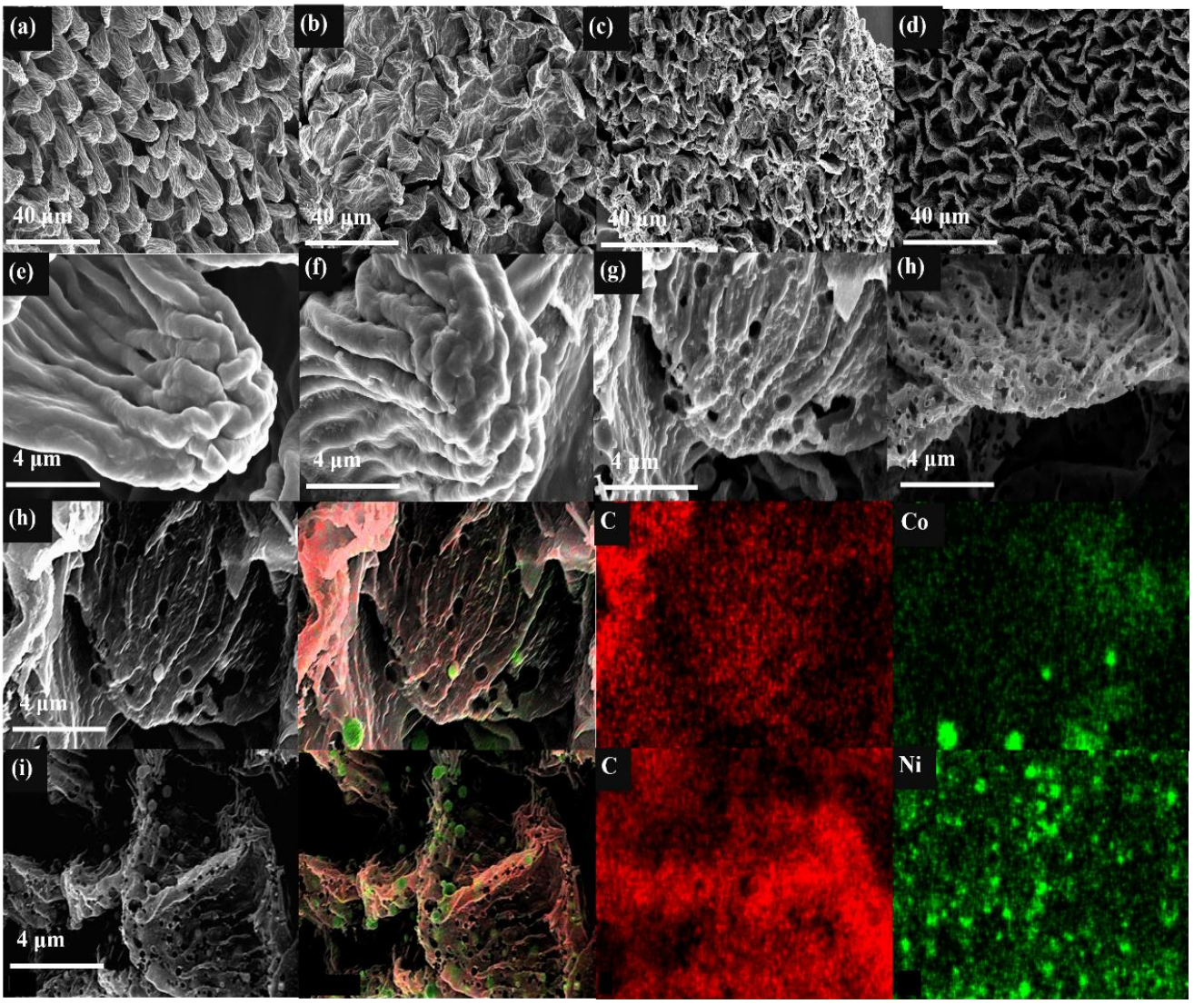

Fig. 4 (a, e) SEM images of raw rose petals; (b, f) raw rose petals after impregnation; (c, g) RC/Co; (d, h) RC/Ni, (h, i) elemental mapping images of RC/Co and RC/Ni.

To clarify the EMW absorption capabilities of the RC/Co and RC/Ni absorber and the impact of proportion and types of nanoparticles on the EMW absorption properties, the electromagnetic parameters of RC/Co and RC/Ni were assessed using complex permittivity and complex permeability, as illustrated in Fig. 6. The real part (ε', μ') of complex permittivity (εr = ε' - iε"), complex permeability (μr = μ' - iμ") are associated with the storage capacity of electromagnetic energy, while the imaginary parts (ε" and μ") signify the loss of electromagnetic energy. As shown in Fig. 6(a), RC/Co have high real part of complex permittivity values (ε′: 20.72-12.17) and high real imaginary of complex permittivity values (ε″: 12.91-1.90). For RC/Ni, it has similar the complex permittivity values (ε′: 23.91-12.05, ε″: 13.70-1.26), indicating a relatively stronger dielectric loss performance. Meanwhile, Fig. 6 depicts RC/Co and RC/Ni have weak μ' and μ", This is due to the low content of cobalt and nickel in the RC/Co and RC/Ni.

Dielectric tangent loss (tanδε = ε″/ε′) and magnetic tangent loss (tanδμ = μ"/μ') are common parameters that characterize the dielectric and magnetic loss abilities of EMW absorbers. As depicted in Figs. 7(a, b), the variations in tanδε and tanδμ are closely associated with ε″ and μ″, respectively. Considering the relationship of absorption properties with tanδε and tanδμ, higher tanδε values imply a significant contribution of dielectric loss to the absorption property in both samples. However, the role of magnetic particles as additional promoters for achieving better impedance matching is noteworthy, contributing to the overall EMW absorption performance.

The dielectric loss mechanisms of RC/Co and RC/Ni was evaluated using the Cole-Cole plots, as shown in Figs. 7(c, d). For RC/Co and RC/Ni, the Cole-Cole curve was deformed several semicircles, which indicated that there was interface polarization, and dipole polarization in the absorbing process. Besides, straight line appears at the end of all the three Cole-Cole curves, which indicated that there existed conductance loss during microwave absorption process except for

 © Engineered Science Publisher LLC 2024

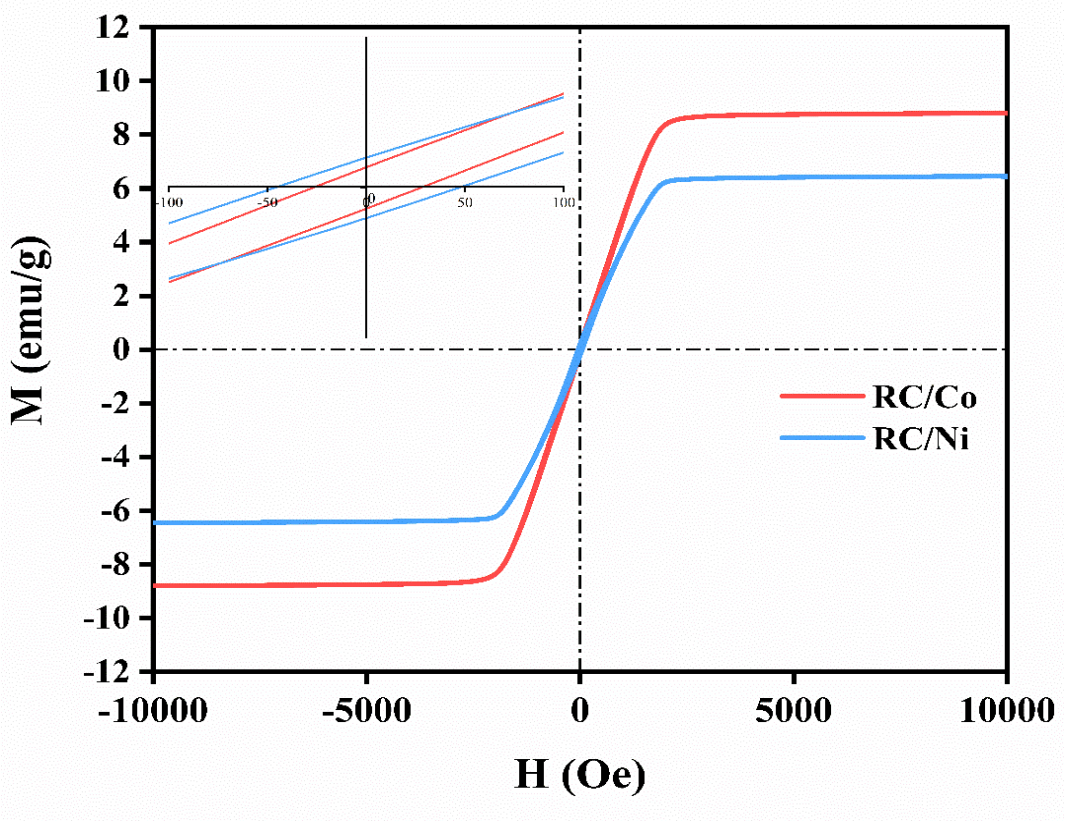

Fig. 5 M-H loops of RC/Co and RC/Ni.

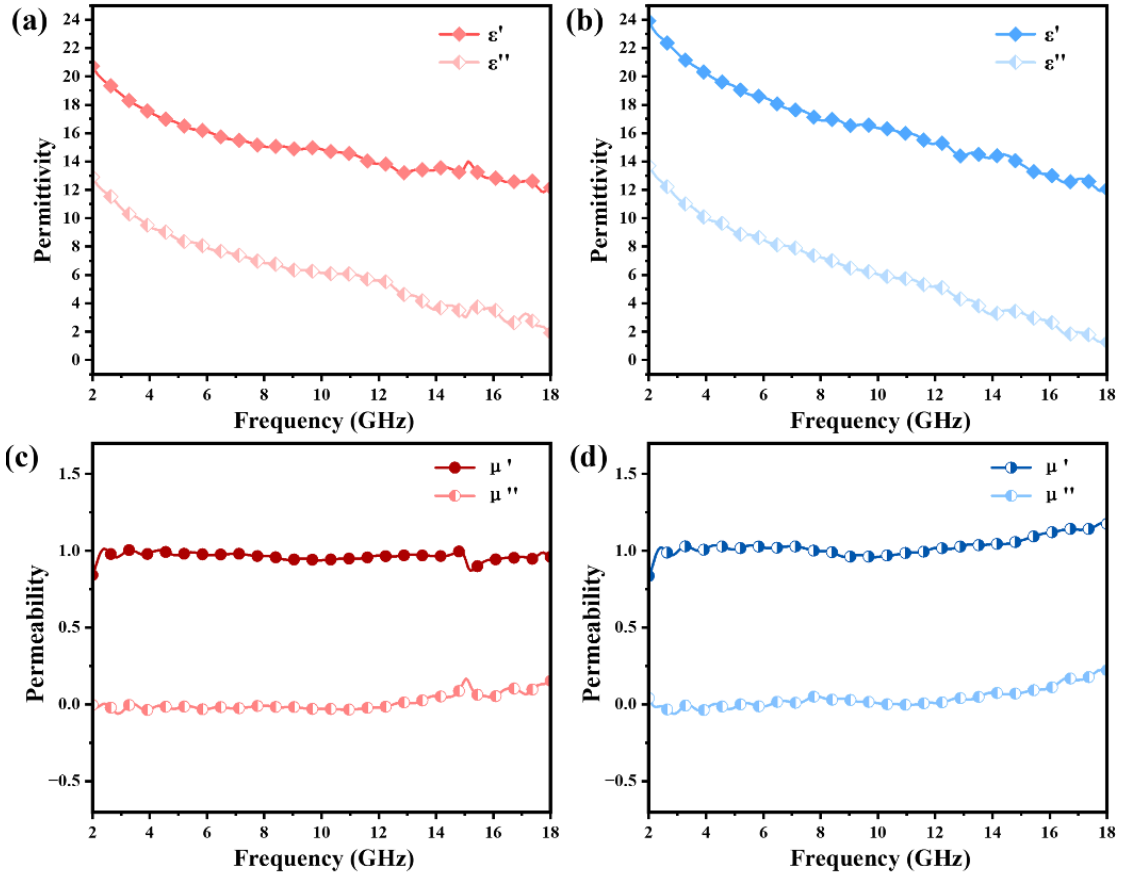

Fig. 6 (a, b) Relative permittivity for RC/Co and RC/Ni absorber at 35% absorber content; (c, d) Relative permeability for RC/Co and RC/Ni absorber at 35% absorber content.

© Engineered Science Publisher LLC 2024

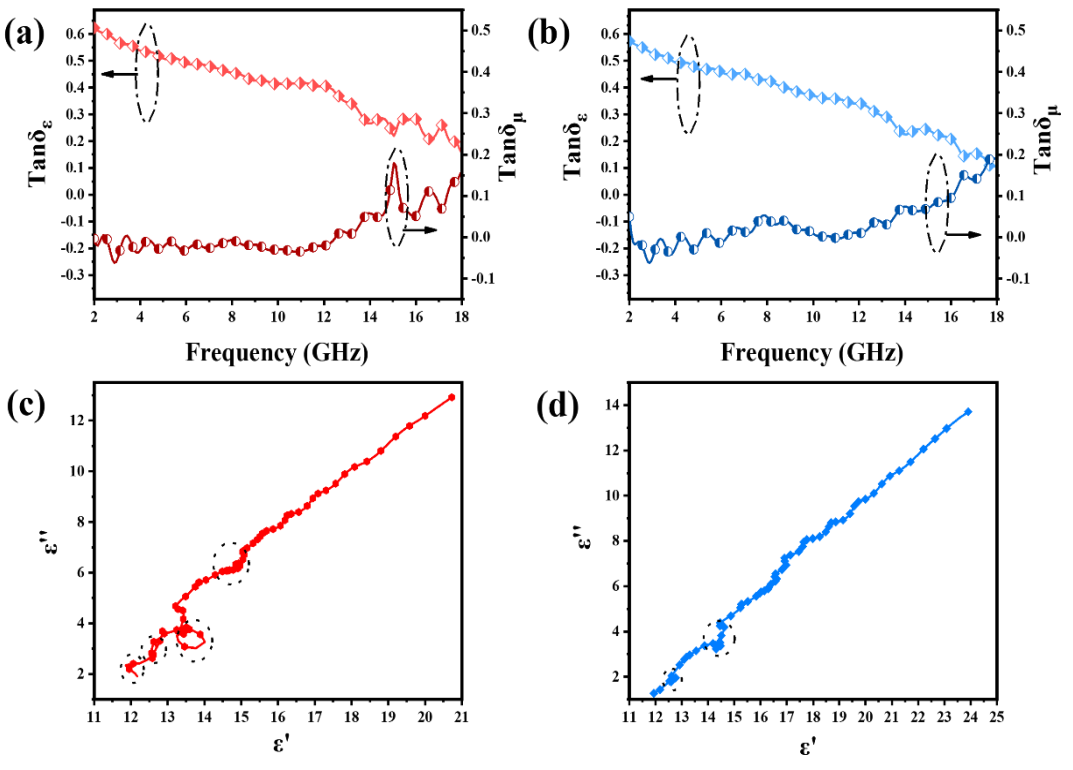

Fig. 7 (a, b) Dielectric tangent loss and magnetic tangent loss of RC/Co and RC/Ni absorber at 35% absorber content; (c, d) Typical Cole-Cole semicircles ε″ versus ε' of RC/Co and RC/Ni absorber at 35% absorber content.

polarization relaxation processes.

The reflection factor (RL), as a function that can directly characterize the EMW absorption performance of RC/Co and RC/Ni, theoretically derived from obtained electromagnetic parameters. According to the transmission line theory, RL can be calculated using the following equations (1) and (2)[32,33]

$$RL = 20\lg\left|\frac{Z_{in}-Z_0}{Z_{in}+Z_0}\right| \quad (1)$$

$$Z_{in} = Z_0\sqrt{\mu_r/\varepsilon_r}tanh\left[j(2\pi fd/c)\sqrt{\mu_r/\varepsilon_r}\right] \quad (2)$$

where Z_{in} represents the equivalent input resistance of the sample; Z_0 represents the impedance of free space, is equal to 377 Ω. The μr and εr are the complex permeability and complex permittivity of the sample, and the c is the speed of

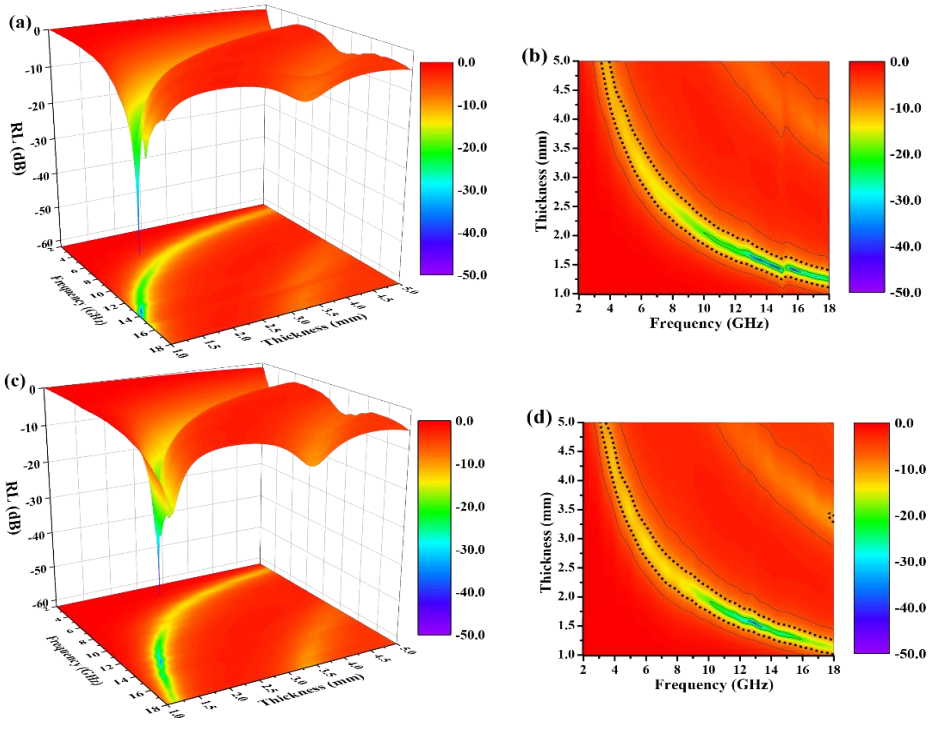

Fig. 8 (a, b) 3D Reflection loss and (c, d) 2D projection plots of RC/Co and RC/Ni.

© Engineered Science Publisher LLC 2024

light in vacuums. f is the frequency; d is the thickness of the specimen. According to the above formula, the RL values of RC/Co and RC/Ni in the thickness range of 1.0-5.0 mm are shown in Fig. 8.

As show at Fig. 8 and Figs. 9(a, b), RC/Co with 1.58 mm thickness obtain minimum reflection loss (RL_{min}) of -47.89 dB (Nearly 99.999% EMW absorption rate) at 13.60 GHz and effective absorption bandwidth (EABW, the RL＜−10 dB, more than 90% EMW absorption) of 4.08 GHz. By comparison, RC/Ni display excellent EMW absorption performance in terms of RLmin and EABW. RC/Ni with 1.56 mm thickness, has the strongest electromagnetic wave loss ability at 12.88 GHz with RLmin of −45.26 dB and EABW is 3.02 GHz. Both RC/Co and RC/Ni show a broadband absorption characteristic.

Following the single-layer homogeneous absorber model, The incident electromagnetic wave that is about to come into contact with the surface of the absorber layer has three directions for its electromagnetic energy (E0) after entering the interior of the absorber layer: Part of E0 reflects on the surface of the layer (air-absorber interface) and returns to the air again the reflected EMW energy on the (E1); Attenuation after entering the interior of absorber the and interacting with it (E2); and the final EMW energy penetrating the absorber layer and re-reflecting on the surface of the the absorber-metal interface (E3). Specifically, When the absorption layer has an appropriate thickness, i.e. a quarter of the incident wavelength frequency, the phase difference between E1 (incident from air-absorber interface) and E3 (ejection from absorber-metal interface) is exactly 180°, so the electromagnetic wave energy of the two can nullify each other. This phenomenon is widely known as the quarter-wavelength cancellation model. Consequently, the absorber layer at a specific thickness (tm) can achieve minimal reflection at a certain EMW frequency (fm). The mathematical relationship between tm and fm satisfy the following equation (3).[34]

$$t_m = \frac{nc}{4f_m\sqrt{|\mu_r||\varepsilon_r|}} \quad (n = 1,3,5\ldots) \tag{3}$$

where the fm is the frequency corresponding to obtaining the RLmin value.

The model portrays the inverse relation between the peak frequency and the absorber layer's thickness. As shown in Figs. 9(b, e), It is expected that all thickness related to RLmin value (red symbols) are located around the blue line (the 1/4 wavelength curve of the peak frequency). Consequently, the RC/Co and RC/Ni obeys the quarter-wavelength cancellation model, and thus can be concluded that RC/Co and RC/Ni has considerable contributions to the EMW attenuation performance.

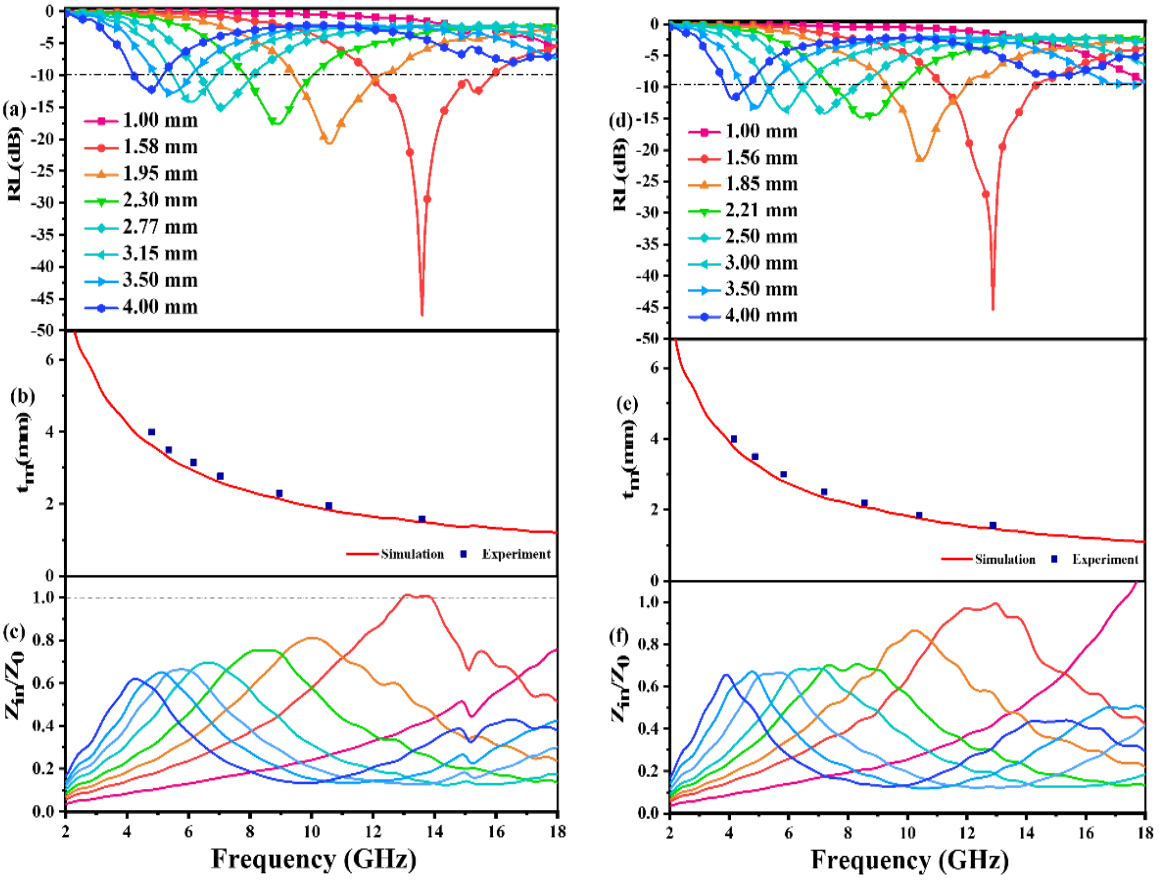

Fig. 9 (a, d) RL curves with different thicknesses of RC/Co and RC/Ni; (b, e) simulated and experimental values under 1/4 wavelength matching conditions of RC/Co and RC/Ni; (c, f) impedance matching characteristics values of RC/Co and RC/Ni.

© Engineered Science Publisher LLC 2024

Besides, to obtain the excellent EMW absorption performance, reducing the reflection of EMW (E1) at the air-absorber interface and improving the absorption of the incident EMW (E2) in the absorber layer with a low reflection at the absorber-metal interface (E3) is necessary. The impedance matching characteristics (Z) is a parameter which characterized the reflection of EMW at the air-absorber interface and is expressed in the following equation (4)[35]

$$Z = |Z_{in}/Z_0| = \sqrt{\mu_r/\varepsilon_r}\tanh\left[j(2\pi fd/c)\sqrt{\mu_r/\varepsilon_r}\right] \quad (4)$$

The frequency dependence of Z for RC/Co and RC/Ni is shown in Figs. 9(c, f). For RC/Co and RC/Ni, at thicknessesof 1.58 and 1.56 mm in the absorber layer, respectively, Z is 1.0006 and 0.9971 at 13.60 and 12.88 GHz, respectively. Simultaneously, these frequencies correspond to the observation of a RLmin. Interestingly, the porous structuresare equivalent to introducing dispersed phases (air) into a continuous phase (carbon), which helps decrease the effective permittivity while balancing permittivity and permeability. Consequently, EMW can easily penetrate the absorber and undergo attenuation rather than reflecting at the absorber surface. Moreover, the well-tuned impedance matching condition of RC/Co and RC/Ni contributes to its outstanding absorbing performance.

4. Conclusions

In this study, rose-derived porous carbon, and Co/Ni nanoparticles composite (RC/Co and RC/Ni) were successfully prepared through an impregnation and one-step pyrolysis process. The unique wrinkled structure on the surface of rose petals and the pores obtained after carbonization jointly increase the specific surface area and significantly contributes to multiple reflection, and strong interfacial polarization of the material. Moreover, the exit of Co and Ni nanoparticle-induced magnetic loss and more interface polarization which enhanced impedance matching condition and EMW dissipation ability of the RC/Co and RC/Ni EMW absorbers.

At a matching thickness of 1.58 mm, RC/Co exhibits RL_{min} of -47.78 dB and an EABW of 4.08 GHz, while RC/Ni exhibits RL_{min} of -45.78 dB and an EABW of 3.78 GHz. Hence, as designed in this study, RC/Co and RC/Ni could offer a low-cost and simple preparation model for synthesizing other high-performance absorbers, effectively mitigating electromagnetic wave-induced pollution.

Acknowledgments

The authors gratefully acknowledge the National Key R&D Program of China (No.2020YFB0408100), Guangdong Innovative and Entrepreneurial Research Team Program (No.2016ZT06C412), National Natural Science Foundation of China (NSFC; No. U20A20340).

Conflict of Interest

There is no conflict of interest.

Supporting Information

Applicable.

References

[1] Y. Li, B. Shen, X. Pei, Y. Zhang, D. Yi, W. Zhai, L. Zhang, X. Wei and W. Zheng, Ultrathin carbon foams for effective electromagnetic interference shielding, *Carbon*, 2016, **100**, 375-385, doi: 10.1016/j.carbon.2016.01.030.

[2] H. Wei, Z. Zhang, G. Hussain, L. Zhou, Q. Li and K. Ostrikov, Techniques to enhance magnetic permeability in microwave absorbing materials, *Applied Materials Today*, 2020, **19**, 100596, doi: 10.1016/j.apmt.2020.100596.

[3] Z. Jia, D. Lan, K. Lin, M. Qin, K. Kou, G. Wu, H. Wu, Progress in low-frequency microwave absorbing materials, *Journal of Materials Science: Materials in Electronics*, 2018, **29**, 17122, doi: 10.1007/s10854-018-9909-z.

[4] O. P. Gandhi, Electromagnetic fields: human safety issues, *Annual Review of Biomedical Engineering*, 2002, **4**, 211-234, doi: 10.1146/annurev.bioeng.4.020702.153447.

[5] J. Huang, D. Sun, J.-K. Wang, Prospects for the application of artificially cultured diatom materials in energy and environment, *ES Energy & Environment*, 2020, **8**, 3-4, doi: 10.30919/esee8c486.

[6] W. Hou, K. Peng, S. Li, F. Huang, B. Wang, X. Yu, H. Yang, H. Zhang, Designing flower-like MOFs-derived N-doped carbon nanotubes encapsulated magnetic NiCo composites with multi-heterointerfaces for efficient electromagnetic wave absorption, *Journal of Colloid and Interface Science*, 2023, **646**, 265-274, doi: 10.1016/j.jcis.2023.05.049.

[7] B. Wen, H. Yang, Y. Lin, L. Ma, Y. Qiu and F. Hu, Controlling the heterogeneous interfaces of S, Co co-doped porous carbon nanosheets for enhancing the electromagnetic wave absorption, *Journal of Colloid and Interface Science*, 2021, **586**, 208-218, doi: 10.1016/j.jcis.2020.10.085.

[8] N. Poudyal, C. Rong, Y. Zhang, D. Wang, M. J. Kramer, R. J. Hebert, J. Ping Liu, Self-nanoscaling in FeCo alloys prepared via severe plastic deformation, *Journal of Alloys and Compounds*, 2012, **521**, 55-59, doi: 10.1016/j.jallcom.2012.01.026.

[9] D. Huang, J. Dai, Q. Wang, H. Liu, Z. Li, MWCNTs wrapped in hollow with open holes of $CoFe_2O_4$ as high-performance electromagnetic wave absorbers, *Journal of Alloys and Compounds*, 2023, **944**, doi: 10.1016/j.jallcom.2023.169194.

[10] X. Li, Y. Sun, Y. Zong, Y. Wei, X. Liu, X. Li, Y. Peng and X. Zheng, Size-effect induced cation redistribution on the magnetic properties of well-dispersed $CoFe_2O_4$ nanocrystals, *Journal of Alloys and Compounds*, 2020, **841**, 155710, doi: 10.1016/j.jallcom.2020.155710.

[11] M. Qin, L. Zhang, H. Wu, Dual-template hydrothermal synthesis of multi-channel porous $NiCo_2O_4$ hollow spheres as high-performance electromagnetic wave absorber, *Applied Surface Science*, 2020, **515**, 146132, doi: 10.1016/j.apsusc.2020.146132.

 © Engineered Science Publisher LLC 2024

[12] Z. Li, H. Lin, S. Ding, H. Ling, T. Wang, Z. Miao, M. Zhang, A. Meng, Q. Li, Synthesis and enhanced electromagnetic wave absorption performances of Fe_3O_4@C decorated walnut shell-derived porous carbon, *Carbon*, 2020, **167**, 148-159, doi: 10.1016/j.carbon.2020.05.070.
[13] J. Liu, L. Zhang, H. Wu and D. Zang, Boosted electromagnetic wave absorption performance from vacancies, defects and interfaces engineering in Co(OH)F/$Zn_{0.76}Co_{0.24}S$/Co_3S_4 composite, *Chemical Engineering Journal*, 2021, **411**, 128601, doi: 10.1016/j.cej.2021.128601.
[14] B. Quan, X. Liang, G. Ji, Y. Cheng, W. Liu, J. Ma, Y. Zhang, D. Li, G. Xu, Dielectric polarization in electromagnetic wave absorption: Review and perspective, *Journal of Alloys and Compounds*, 2017, **728**, 1065-1075, doi: 10.1016/j.jallcom.2017.09.082.
[15] Q. Li, J. Liu, Y. Zhao, X. Zhao, W. You, X. Li, R. Che, "Matryoshka Doll"-Like CeO_2 Microspheres with Hierarchical Structure To Achieve Significantly Enhanced Microwave Absorption Performance, *ACS Applied Materials & Interfaces*, 2018, **10**, 27540-27547, doi: 10.1021/acsami.8b10353.
[16] Z. Yan, J. Luo, Effects of Ce Zn co-substitution on structure, magnetic and microwave absorption properties of nickel ferrite nanoparticles, *Journal of Alloys and Compounds*, 2017, **695**, 1185-1195, doi: 10.1016/j.jallcom.2016.08.333.
[17] C. Wei, L. Shi, M. Li, M. He, M. Li, X. Jing, P. Liu, J. Gu, Hollow engineering of sandwich NC@Co/NC@MnO_2 composites toward strong wideband electromagnetic wave attenuation, *Journal of Materials Science & Technology*, 2024, **175**, 194-203, doi: 10.1016/j.jmst.2023.08.020.
[18] W.-Y. Li, M.-Y. Gao, Y. Miao, X.-M. Wang, Recent progress in increasing the electromagnetic wave absorption of carbon-based materials, *New Carbon Materials*, 2023, **38**, 111-125, doi: 10.1016/s1872-5805(23)60703-6.
[19] F. Ruiz-Perez, S. M. López-Estrada, R. V. Tolentino-Hernández, F. Caballero-Briones, Carbon-based radar absorbing materials: a critical review, *Journal of Science: Advanced Materials and Devices*, 2022, **7**, 100454, doi: 10.1016/j.jsamd.2022.100454.
[20] M. Zhang, H. Ling, S. Ding, Y. Xie, T. Cheng, L. Zhao, T. Wang, H. Bian, H. Lin, Z. Li, A. Meng, Polyaniline-decorated carbon fibers for enhanced mechanical and electromagnetic interference shielding performances of epoxy composites, *Carbon*, 2021, **174**, 248-259, doi: 10.1016/j.carbon.2020.12.005.
[21] R. Qiang, Y. Du, Y. Wang, N. Wang, C. Tian, J. Ma, P. Xu, X. Han, Rational design of yolk-shell C@C microspheres for the effective enhancement in microwave absorption, *Carbon*, 2016, **98**, 599-606, doi: 10.1016/j.carbon.2015.11.054.
[22] W. Yu, Y. Min, J. Fang, X. Lu, Z. Wang, L. Jian, Polyimide-derived porous carbon/Co particle-based composites for high-performance microwave absorption, *RSC Advances*, 2022, **12**, 29070-29077, doi: 10.1039/d2ra04653a.
[23] F. Li, Z. Bi, H. Kimura, H. Li, L. Liu, X. Xie, X. Zhang, J. Wang, X. Sun, Z. Ma, W. Du, C. Hou, Energy- and cost-efficient salt-assisted synthesis of nitrogen-doped porous carbon matrix decorated with nickel nanoparticles for superior electromagnetic wave absorption, *Advanced Composites and Hybrid Materials*, 2023, **6**, 133, doi: 10.1007/s42114-023-00710-8.
[24] H.-C. Zhang, C.-N. Yu, X.-Z. Li, L.-F. Wang, J. Huang, J. Tong, Y. Lin, Y. Min, Y. Liang, Recent developments of nanocellulose and its applications in polymeric composites, *ES Food & Agroforestry*, 2022, **9**, 1-14, doi: 10.30919/esfaf768.
[25] D. Wei, M. Weng, M. H. H. Mahmoud, A. Y. Elnaggar, I. H. El Azab, X. Sheng, M. Huang, Z. M. El-Bahy, J. Huang, Development of novel biomass hybrid aerogel supported composite phase change materials with improved light-thermal conversion and thermal energy storage capacity, *Advanced Composites and Hybrid Materials*, 2022, **5**, 1910-1921, doi: 10.1007/s42114-022-00519-x.
[26] M. Weng, S. Liu, J. Su, W. Xu, J. Huang, W. Tan, Y. Liu and Y. Min, Hydrophobic and antimicrobial polyimide based composite phase change materials with thermal energy storage capacity, applied as multifunctional construction material, *Engineered Science*, 2022, **19**, 301-311, doi: 10.30919/es8e735.
[27] W. T. Cao, F. F. Chen, Y. J. Zhu, Y. G. Zhang, Y. Y. Jiang, M. G. Ma, F. Chen, Binary strengthening and toughening of mxene/cellulose nanofiber composite paper with nacre-inspired structure and superior electromagnetic interference shielding properties, *ACS Nano*, 2018, **12**, 4583-4593, doi: 10.1021/acsnano.8b00997.
[28] R. Zhang, J. Qiao, X. Zhang, Y. Yang, S. Zheng, B. Li, W. Liu, J. Liu, Z. Zeng, Biomass-derived porous carbon for microwave absorption, *Materials Chemistry and Physics*, 2022, **289**, 126437, doi: 10.1016/j.matchemphys.2022.126437.
[29] J. Fang, P. Li, Y. Liu, Y. Min, Cobalt magnetic particles and carbon composite microtubes as high-performance electromagnetic wave absorbers, *Journal of Materials Chemistry C*, 2021, **9**, 2474-2482, doi: 10.1039/d0tc05409g.
[30] T. Hou, Z. Jia, S. He, Y. Su, X. Zhang, B. Xu, X. Liu, G. Wu, Design and synthesis of NiCo/Co_4S_3@C hybrid material with tunable and efficient electromagnetic absorption, *Journal of Colloid and Interface Science*, 2021, **583**, 321-330, doi: 10.1016/j.jcis.2020.09.054.
[31] T. Zhao, C. Hou, H. Zhang, R. Zhu, S. She, J. Wang, T. Li, Z. Liu, B. Wei, Electromagnetic wave absorbing properties of amorphous carbon nanotubes, *Scientific Reports*, 2014, **4**, 5619. 10.1038/srep05619.
[32] Z. Wang, Y. Min, J. Fang, W. Yu, W. Huang, X. Lu, B. Wang, Polyimide aerogel-derived amorphous porous carbon/crystalline carbon composites for high-performance microwave absorption, *RSC Advances*, 2023, **13**, 7055-7062, doi: 10.1039/d3ra00155e.
[33] T. Zhao, Z. Jia, Y. Zhang, G. Wu, Multiphase Molybdenum carbide doped carbon hollow sphere engineering: the superiority of unique double-shell structure in

© Engineered Science Publisher LLC 2024

microwave absorption, *Small*, 2023, **19**, 2206323, doi: 10.1002/smll.202206323.
[34] D. Wang, J. Jin, Y. Guo, H. Liu, Z. Guo, C. Liu, C. Shen, Lightweight waterproof magnetic carbon foam for multifunctional electromagnetic wave absorbing material, *Carbon*, 2023, **202**, 464-474, doi: 10.1016/j.carbon.2022.11.019.
[35] S. Zhang, Z. Jia, Y. Zhang and G. Wu, Electrospun $Fe_{0.64}Ni_{0.36}$/MXene/CNFs nanofibrous membranes with multicomponent heterostructures as flexible electromagnetic wave absorbers, *Nano Research*, 2022, **16**, 3395-3407, doi: 10.1007/s12274-022-5368-1.

Publisher's Note: Engineered Science Publisher remains neutral with regard to jurisdictional claims in published maps and institutional affiliations.

© Engineered Science Publisher LLC